BASIC SCIENCE

Nanomedicine: Nanotechnology, Biology, and Medicine
14 (2018) 1879–1889

Research Article

nanomedjournal.com

Dendritic PEG outer shells enhance serum stability of polymeric micelles

Hao-jui Hsu, PhD[a,b], Yanxiao Han, BS[c], Michael Cheong, BS[b], Petr Král, PhD[c,d,*], Seungpyo Hong, PhD[a,b,e,**]

[a]*Pharmaceutical Sciences Division, School of Pharmacy, University of Wisconsin, Madison, WI*
[b]*Department of Biopharmaceutical Sciences, University of Illinois at Chicago, Chicago, IL*
[c]*Department of Chemistry, University of Illinois at Chicago, Chicago, IL*
[d]*Department of Physics, University of Illinois at Chicago, Chicago, IL*
[e]*Yonsei Frontier Lab and Department of Pharmacy, Yonsei University, Seoul*

Received 8 January 2018; accepted 4 May 2018

Abstract

A higher surface density of poly(ethylene glycol) (PEG) on polymeric micelles enhances their stability in serum, leading to improved plasma circulation. To obtain fundamental, mechanistic understanding of the PEG effect associated with polymeric architecture/configuration, we have synthesized PEGylated dendron-based copolymers (PDCs) and linear block copolymers (LBCs) with similar molecular weights. These copolymers formed dendron (hyperbranched) and linear micelles, respectively, which were compared in terms of their stabilities in serum, micelle-serum protein interactions, and *in vivo* biodistributions. Overall, the dendron micelles exhibited a better serum stability (longer half-life) and thus a slower release profile than the linear micelles. Fluorescence quenching assays and molecular dynamics (MD) simulations revealed that the high serum stability of the dendron micelles can be attributed to reduced micelle-serum protein interactions, owing to their dendritic, dense PEG outer shell. These results provide an important design cue for various polymeric micelles and nanoparticles.

Key words: Dendritic nanoparticles; PEG; Dendron micelles; Nano-bio interactions; Serum stability

A variety of polymeric nanoparticles (NPs) have been widely employed as potential drug delivery vehicles for therapeutic and diagnostic agents.[1–4] Although many NPs have demonstrated efficient tumor targeting holding promise as potential anti-cancer therapy,[5,6] numerous challenges, particularly with regard to achieving controllable nano-bio interactions, still remain to be addressed.[7,8] An important challenge negatively affecting the performance of nanocarriers (NCs) is the NPs-serum protein interactions. As the NCs enter the systematic circulation, serum proteins could rapidly adsorb onto their surfaces in a form of "protein corona".[9,10] This uncontrolled NPs-protein interaction can trigger opsonization-mediated NPs uptake by immune cells, disturbing the pharmacokinetic properties of NCs.[11] The adsorbed protein corona can also block the targeting ligands attached on the NPs surface and diminish the specificity of the targeted NPs.[12–14]

For micelle-based NCs, the consequences of such serum protein interactions could be destructive. After being adsorbed on the micelle surface, the serum proteins could penetrate the hydrophobic micelle core, extract hydrophobic molecules from it, and eventually disintegrate the micelles.[11] These undesirable interactions could fail the micellar NCs to deliver their incorporated drug molecules to the intended sites and tissue *in vivo*.[11,15,16] Thus, reducing the micelle-serum protein interactions would substantially improve the effectiveness of these self-assembled NCs.[16] One of the most commonly used strategies in these efforts is to introduce a highly hydrophilic polymer, such as poly(ethylene glycol) (PEG), to the surface of the micelles.[17–19] The PEG outer shell decreases the protein adsorption, helps NCs to avoid recognition by the immune system, and thus prolong their circulation time.[20,21] Typically, PEG is conjugated to a linear hydrophobic polymer, resulting in

*Correspondence to: P. Král, Department of Chemistry, The University of Illinois at Chicago, 845 W. Taylor St., Chicago, IL 60607.

**Correspondence to: Seungpyo Hong, Division of Pharmaceutical Sciences, School of Pharmacy, The University of Wisconsin-Madison, 777 Highland Ave., Madison, WI 53705.

E-mail addresses: pkral@uic.edu (P. Král), seungpyo.hong@wisc.edu (S. Hong).

https://doi.org/10.1016/j.nano.2018.05.010
1549-9634/

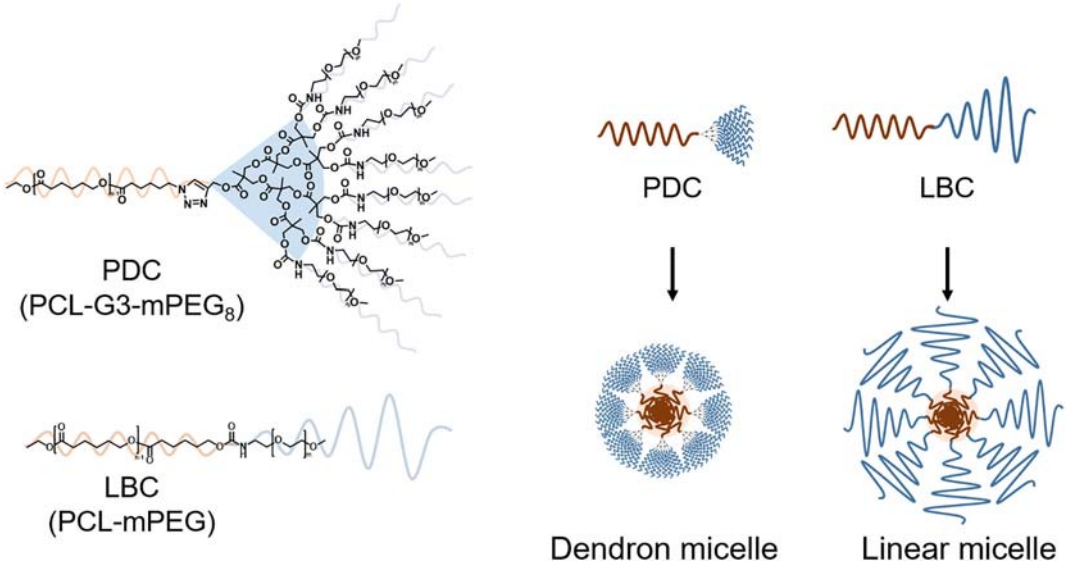

Figure 1. Schematic illustration of the structural difference between PEGylated dendron-based copolymer (PDC) and linear block copolymer (LBC).

a linear amphiphilic copolymer that forms a self-assembled micelle.[16] However, this linear configuration often results in less dense PEG outer shell, which could provide limited protection to the micelles.[22,23]

The dendritic amphiphilic copolymers tested in this study were developed by our group. The PEGylated dendron-based copolymers (PDCs) consist of hydrophilic poly(ε-caprolactone) (PCL), polyester dendron, and multiple hydrophilic PEG chains (Figure 1).[24] Due to their conical structure, these amphiphilic PDCs could self-assemble into dendron micelles with enhanced thermodynamic stability. The critical micelle concentrations (CMCs) of those dendron micelles were ranged from 10^{-7} to 10^{-8} M, which were up to two orders of magnitude lower than those of similar linear block copolymers (LBCs). More importantly, our molecular dynamics (MD) simulations proved that the dendritic architecture of PDCs formed a high-density PEG outer shell on the self-assembled micelles. The high-density PEG outer shell is expected to reduce the undesired interactions of the dendron micelles with biological components. Based on these findings, we have demonstrated that the high-density PEG layer of dendron micelles does reduce the uncontrolled drug release to non-targeted cells[22] However, the effects of this design on micelle-serum protein interactions have not been investigated.

To systematically study the effects of the dendritic PEG outer shell on the micelle-serum protein interactions, we synthesized PDCs and LBCs with similar molecular weight and hydrophilic lipophilic balance (HLB) and compared their serum stabilities, micelle-serum protein interactions, and *in vivo* biodistributions. Our results obtained from a series of both experimental and theoretical investigations help us better understand the potential of manipulating polymer architecture to enhance the performance of self-assembled NCs in physiological environments, providing critical design cues for developing effective micellar NCs.

Methods

Materials, synthesis of PDCs and LBCs and micelle preparation

PDCs and LBCs were synthesized and self-assembled into micelles according to our published protocols.[22,24,25] The complete synthesis/preparation methods, along with characterization methods, can be found in the supporting information.

Stability of DMs and LMs measured using FRET

FRET-micelles were incubated in PBS buffer or 50% FBS at a concentration of 100 μg/mL. The samples were incubated up to 48 h at 37 °C with gentle agitation. The emission spectra of FRET-micelles were obtained using a fluorescence spectrophotometer (RF 1501, Shimadzu, Japan) set at an excitation wavelength of 484 nm. FRET ratios were calculated as $I_{565}/(I_{565} + I_{510})$. To estimate the half-life of FRET-micelles in 50% serum, a standard curve was made to correlate the FRET ratio and residual micelle fraction (RMF).[26] FRET-LM3.5 K micelles ($PCL_{3.5K}$-$mPEG_{5K}$) were incubated in 50% FBS for 48 h. By assuming all the FRET-LM3.5 K micelles have disassembled under this condition, the disassembled FRET-micelles were mixed with freshly prepared micelles at various concentration ratios. The fluorescence spectra of each micelle mixture were then measured to obtain the FRET ratio. To calculate the disassembly kinetic of micelles, we assumed that the disassembly of micelles follows a first-order kinetic. Therefore, a nonlinear fit using a first-order decay equation (Eq. (1)) was performed to estimate the decay constant of FRET-micelles in 50% FBS. The decay constant could be further converted to the half-life of FRET-micelles using Eq. (2).

$$\mathrm{RMF}_t = \mathrm{RMF}_{t0} \times e^{-kt} \quad (1)$$

Table 1
Theoretical molecular weights, HLBs, and measured molecular weights of PDCs and LBCs.

Polymers	Theoretical MW (g/mol)		HLB*	M_n†
	PCL	PEG		
$PCL_{3.5K}$-$mPEG_{5K}$	3500	5000	11.8	8130
$PCL_{3.5K}$-G3-$mPEG_{0.6K}$	3500	4800	12.4	8234
PCL_{14K}-$mPEG_{5K}$	14,000	5000	5.3	18,717
PCL_{14K}-G3-$mPEG_{0.6K}$	14,000	4800	5.8	19,122

* HLB = $20M_H/(M_H + M_L)$ where M_H: molar mass of hydrophilic segment and M_L: molar mass of lipophilic segment.
† Measured using ^{1}H NMR.

$$t_{1/2} = \frac{ln2}{K} \quad (2)$$

Where RMF is residual micelles fraction, t is time, K is the decay constant and $t_{1/2}$ is the half-life.

In vitro doxorubicin release study

The release profile of doxorubicin (DOX) from the DOX-loaded micelles was evaluated using a dialysis method. 1.5 mL of DOX-loaded micelles (1 mg/mL) were mixed with 1.5 mL of FBS and placed in a dialysis membrane (MWCO 3.5 kDa) to dialyze against 27 mL of 50% FBS at 37 °C with gentle shaking (100 rpm). At predetermined time points, 3 mL dialysate were sampled and replaced by fresh medium. The DOX content in the collected samples were quantified by the fluorescence at 484 nm excitation and 584 nm emission using a fluorescence plate reader. (Gemini XPS, Molecular Devices, CA, USA).

Micelle-serum albumin interactions

The interactions between micelles and bovine serum albumin (BSA) were evaluated by the changes in the intrinsic fluorescence properties of tryptophan within BSA molecules using a fluorescence spectrophotometer (RF 1501, Shimadzu, Japan). The excitation was set at 295 nm and the emission spectra were recorded in the rage of 315–400 nm. BSA stock solution (25 μM) was freshly prepared in PBS buffer. BSA stock solution (0.4 mL) was then added into micelle solutions (1.6 mL) with different polymer concentrations. After 30 min of incubation, the fluorescence spectrums of the micelle-BSA solutions were recorded. To quantify the quenching effect, the fluorescence data were analyzed using the Stern-Volmer equation (Eq. (3)) to calculate the quenching constant of each micelle, where the Stern-Volmer quenching constant is proportional to the level of interactions between the two species.

$$F_0/F = 1 + K_{SV}[Q]. \quad (3)$$

F_0 and F are the BSA fluorescence intensities in the absence and presence of copolymers, respectively, *Ksv* is the Stern-Volmer quenching constant, and [Q] is the concentration of the copolymers.

Table 2
Sizes, surface charges, and CMCs of DMs and LMs.

Micelles	Polymers	Particle size (nm)	Zeta-potential (mV)	CMC ($\times 10^{-7}$ M)
LM3.5 K	$PCL_{3.5K}$-$mPEG_{5K}$	36.29 ± 13.91	−2.75 ± 0.42	3.75
DM3.5 K	$PCL_{3.5K}$-G3-$PEG_{0.6K}$	31.30 ± 9.34	−3.55 ± 0.39	2.85
LM14K	PCL_{14K}-$mPEG_{5K}$	65.30 ± 17.92	−4.20 ± 0.20	0.82
DM14K	PCL_{14K}-G3-$PEG_{0.6K}$	51.41 ± 11.99	−2.17 ± 0.39	0.60

Molecular dynamics (MD) simulations

Atomistic MD simulations of LM3.5 K and DM3.5 K micelle-BSA assemblies were performed in a 150 mM NaCl solution with an aggregation number of N_{agg} = 60. Six BSA proteins with different orientations were placed around each of the LM and DM to simulate their mutual interactions. The systems were simulated with NAMD[27] and the CHARMM force field (CHARMM27[28,29] and CHARMM36[30–32]) in a NPT ensemble at pressure of 1 bar and temperature of 300 K, using Langevin dynamics with a damping constant of 0.01 ps^{-1} and a time step of 2 fs. Long-range electrostatic interactions were calculated by PME[33] in the presence of periodic boundary conditions. The Coulombic and vdW coupling energies between micelle and BSA were calculated by VMD[34] software using a dielectric constant of 80 (screening was not included). Inclusion of screening would decrease Coulombic coupling, but preserve the much larger vdW coupling and thus the qualitative picture (stronger protein-micelle coupling in LM3.5 K).

In vivo biodistribution study

6–8 weeks old BALB/c female mice were obtained from Charles River Laboratory. Each mouse was anesthetized by ketamine/xylazine (50 mg/kg and 5 mg/kg, respectively) prior to receiving a tail vein injection of the dual-labeled micelles suspended in PBS at a dose of 10 mg/kg. At 4 and 24-h post-injection, the animals were euthanized with ketamine/xylazine (100 mg/kg and 10 mg/kg, respectively). Their blood was then collected by cardiac puncture using a 25 gauge needle and 1 mL syringe and stored in EDTA-coated tubes at 4 °C until analysis. As an additional insurance of death, cervical dislocation was performed and the major organs (heart, kidney, liver, lung, and spleen) were harvested, washed by 1X PBS and then frozen until analysis. For the sample processing, the collected blood samples were centrifuged at 3000 rpm for 5 min to remove hematological cells before analysis. The organ samples were carefully weighted and then homogenized in 50% DMSO (three-fold volume to the tissue weight) followed by centrifugation at 16,000 × g for 20 min. The serum samples and the supernatants of tissue samples were measured fluorometrically to determine the amounts of rhodamine and DiO in each of the sample. Regression curves of dual-labeled DMs and LMs in each tissue were prepared to convert the fluorescent signals to the percentages of the initial injected dose. The biodistribution data was presented in percent of initial dose per g tissue.

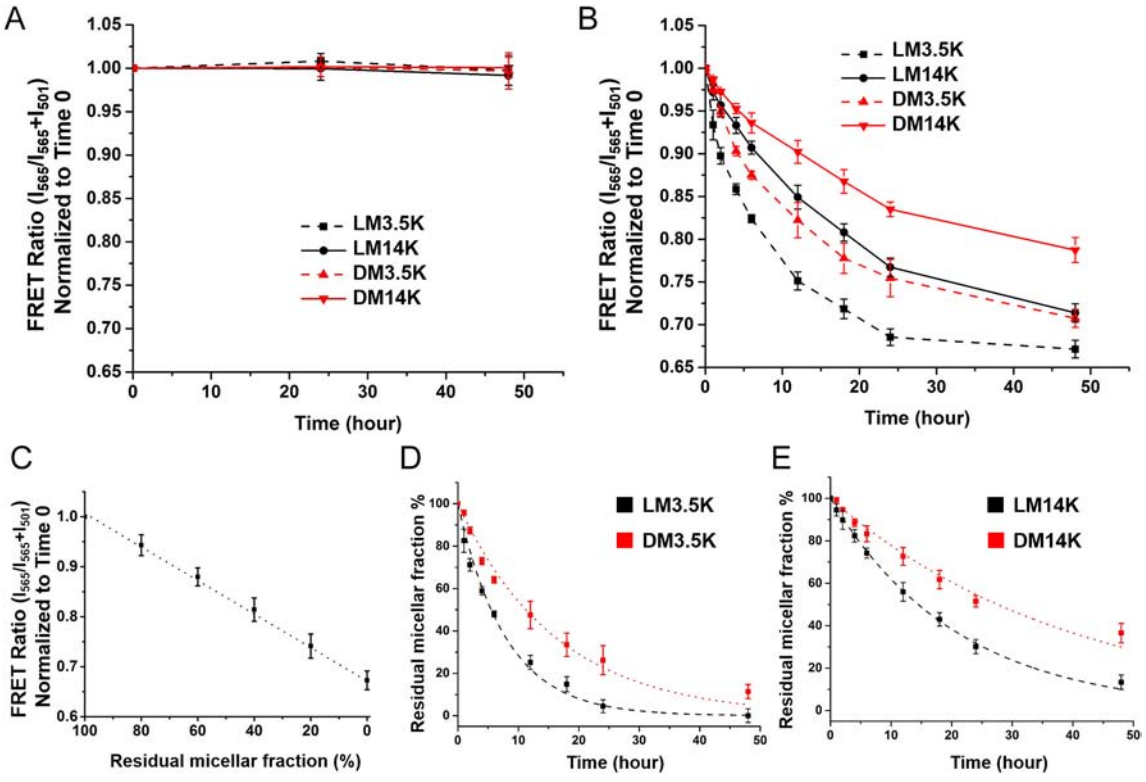

Figure 2. Fluorescence measurements of FRET pairs (DiI and DiO) encapsulated in LMs or DMs. Time-dependent FRET ratios ($I_{565}/(I_{565} + I_{501})$), normalized to time 0, in PBS **(A)** and 50% FBS **(B)**. **(C)** Standard curve that correlates FRET ratio to residual micellar fraction. It is assumed that all FRET-LM3.5 K micelles are completely disassembled after incubation in 50% FBS for 48 h. Under this assumption, the observed FRET ratios can be converted into residual micellar fractions. Time-dependent residual micellar fractions of LM3.5 K and DM3.5 K micelles **(D)** and LM14K and DM14K micelles **(F)**. Results are presented as average ± S.D. (n = 3).

Table 3
The calculated half-lives of DMs and LMs in 50% FBS.

Micelles	Half-life in 50% FBS (h)
LM3.5 K	5.51 ± 0.20
DM3.5 K	11.35 ± 1.85
LM14K	14.47 ± 0.52
DM14K	27.71 ± 2.91

Results

Preparation of amphiphilic copolymers and polymeric micelles

To study the effect of dendritic polymer architecture on the micelle-protein interactions, two PDCs ($PCL_{3.5K}$-G3-$mPEG_{0.6K}$ and PCL_{14K}-G3-$mPEG_{14K}$) with different molecular weights were synthesized using the protocol published previously and compared with their liner counterparts ($PCL_{3.5K}$-$mPEG_{5K}$ and PCL_{14K}-$mPEG_{5K}$) (Table 1).[22,24,25] As described in Figure 1, the major difference between PDCs and LBCs is the configuration of their hydrophilic segments. A PDC chain comprises a hydrophilic polyester dendron and eight short PEG chains (600 g/mol) whereas there is only a single long PEG chain (5000 g/mol) in the hydrophilic segment of a LBC chain. With the chosen size of the hydrophobic polymer chain, PCL, each set of the PDCs and LBCs is characterized by their similar total molecular weights and HLBs (Table 1).

The four amphiphilic copolymers self-assembled into dendron and linear micelles through dialysis. The dendron and linear micelle were denoted as DM and LM, respectively, followed by the molecular weight of PCL chain. For example, the dendron micelles made from $PCL_{3.5K}$-G3-$mPEG_{0.6K}$ is denoted as DM3.5 K. The particle sizes, zeta-potentials and critical micelle concentrations (CMCs) of the micelles were measured and summarized in Table 2. The size distribution profiles, along with the polydispersity values, measured using dynamic light scattering (DLS) are also shown in Figure S1. The hydrodynamic diameters of DMs were slightly smaller than those of their linear counterparts, likely due to their shorter PEG corona, although the size distribution remained similar between the two groups. The change in polymer architecture did not significantly alter the aggregation numbers of the micelles, since the particle size measurements by DLS and transmission electron microscopy (TEM) images of the micelles (Figure S2) both suggested that the particle sizes of the micelles were mainly determined by the length of PCL chain, not by their polymer architecture or PEG chain length. The zeta-potentials of the micelles were not noticeably affected by the polymer architecture either, given that all the tested micelles showed slightly negative zeta potential values ranging from −2 to −5 mV. As expected, the use of longer hydrophobic segments of the copolymers lowered the CMCs of the micelles, due to the increasing cohesion of the hydrophobic cores (Table 2).[35,36] With the same length of the hydrophobic

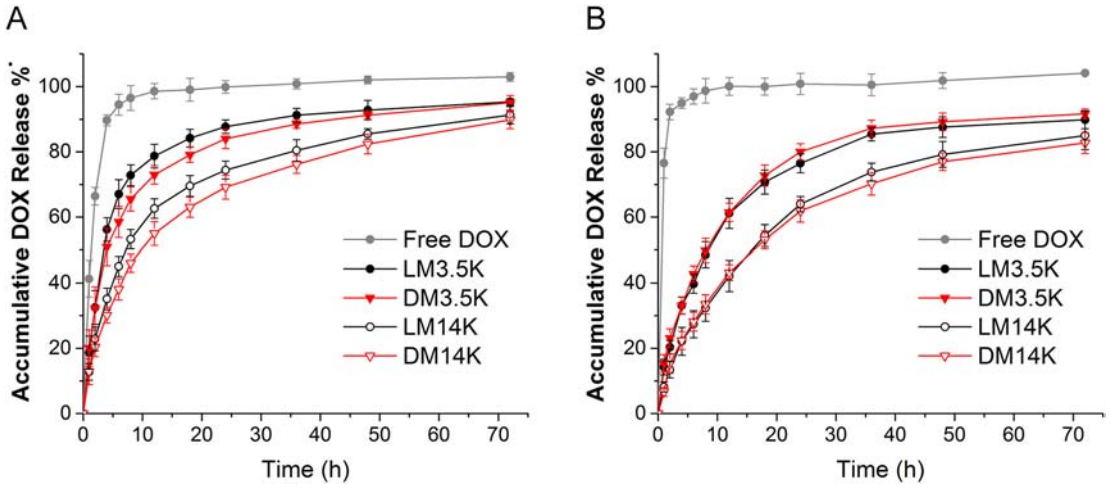

Figure 3. *In vitro* DOX release profiles from DMs and LMs in 50% FBS **(A)**, and 1% Tween 80 **(B)** using a dialysis method. Results are presented as average ± S.D. (n = 3).

segment, DMs exhibited lower CMCs than LMs, suggesting a superior thermodynamic stability of DMs that has been reported previously.[24]

Stability of DMs and LMs measured by Förster resonance energy transfer (FRET)

Fluorescence probes have been widely used to study the stability of self-assembled NPs upon interactions with biological components. The Maysinger group first reported that linear PCL-PEG micelles were stable in PBS, but they disassembled in serum-containing medium, as observed using fluorescence-labeled polymers.[37] Recently, several studies using a FRET-based method have reported the instability of polymeric micelles upon their interactions with serum proteins.[15,26,38] This method can also discriminate the serum stability of polymeric micelles with different hydrophobic polymer structures.[39] Typically, this approach uses a FRET pair, *e.g.*, 3,3′-dioctadecylox-acarbocyanine perchlorate (DiO) as the donor and 1,1′-diocta-decyl-3,3,3′,3′-tetramethylindocarbocyanine perchlorate (DiI) as the acceptor, to assess the integrity of micelles. When both dyes are encapsulated in the micelle core, the distance between the two molecules is within a few nanometer range. Under this condition, optical excitation of the FRET donor at 484 nm results in a strong emission of the FRET acceptor at 565 nm, due to the overlapping DiO emission and DiI excitation spectra. In contrast, when the micelles disassemble, the two dye molecules diffuse into the medium and are no longer in a sufficient proximity of each other, resulting in loss of the FRET signal.

Here, the FRET-based technique was employed to compare the serum stability of DMs and LMs. To prepare FRET-micelles, DiO and DiI molecules were encapsulated into DMs or LMs through self-assembly. The stability of these FRET-micelles was first monitored in PBS buffer at 37°C up to 48 hours (Figures 2, *A* and S3). The FRET ratio ($I_{565}/(I_{501} + I_{565})$) of all the micelles tested remained constant throughout 48 hours, showing that all the micelles were stable in the absence of serum proteins. In sharp contrast, in 50% fetal bovine serum (FBS), the FRET ratios of the micelles rapidly decreased over time, indicating the integrity of the micelles was disrupted, as a result of the micelle-serum protein interactions (Figures 2, *B* and S4). The serum stability of the micelles was generally proportional to the length (molecular weight) of the hydrophobic polymer (PCL) chains for both DMs and LMs.[39] Interestingly, with the same molecular weight of the PCL chains, DMs (both DM3.5 K and DM14K) displayed a significantly slower decrease in FRET ratio over 48 hours compared to their LM counterparts (Figures 2, *B* and S4). This enhancement indicates that the incorporation of dendritic polymer architecture could improve the serum stability of the micelles.

In order to quantitatively measure the FRET-micelles integrity, we established a standard curve to convert the FRET ratio of micelles into the residual micelle fraction (RMF).[26] Briefly, the FRET-LM3.5 K micelles were assumed 100% disassembled after 48-h incubation, since the calculated FRET ratio at this time point was similar to the FRET ratio of free DiO/DiI in FBS without micelles.[26] A standard curve that correlates FRET ratio to RMF was established by recording the FRET ratios of micelle mixtures containing 100% disassembled micelles and freshly prepared micelles at various mixing ratios (Figure 2, *C*). After converting the calculated FRET ratios of micelle to RMF, a non-linear curve fitting was performed to estimate the half-life of the micelles (Figure 2, *D* and *E*). When a first order decay equation (Eq. (1), see the methods section) was employed for the curve fitting, a good correction was observed ($R^2 > 0.90$) for all the micelles, indicating that the micelle disintegration followed a first order kinetic profile. The estimated half-lives of DMs and LMs were calculated using Eq. (2) (see the methods section) and presented in Table 3. The size of the hydrophobic segment is clearly a major factor that affects the half-life of micelles in serum, *i.e.*, the longer PCL block, the longer half-life of the micelles. Notably, the incorporation of dendritic architecture significantly prolongs the half-life of the micelles as well. The half-life of DMs was approximately 2-fold longer than that of LM counterparts. Therefore, the short, dense PEG outer shell formed by PDCs could mitigate the micelle-serum protein

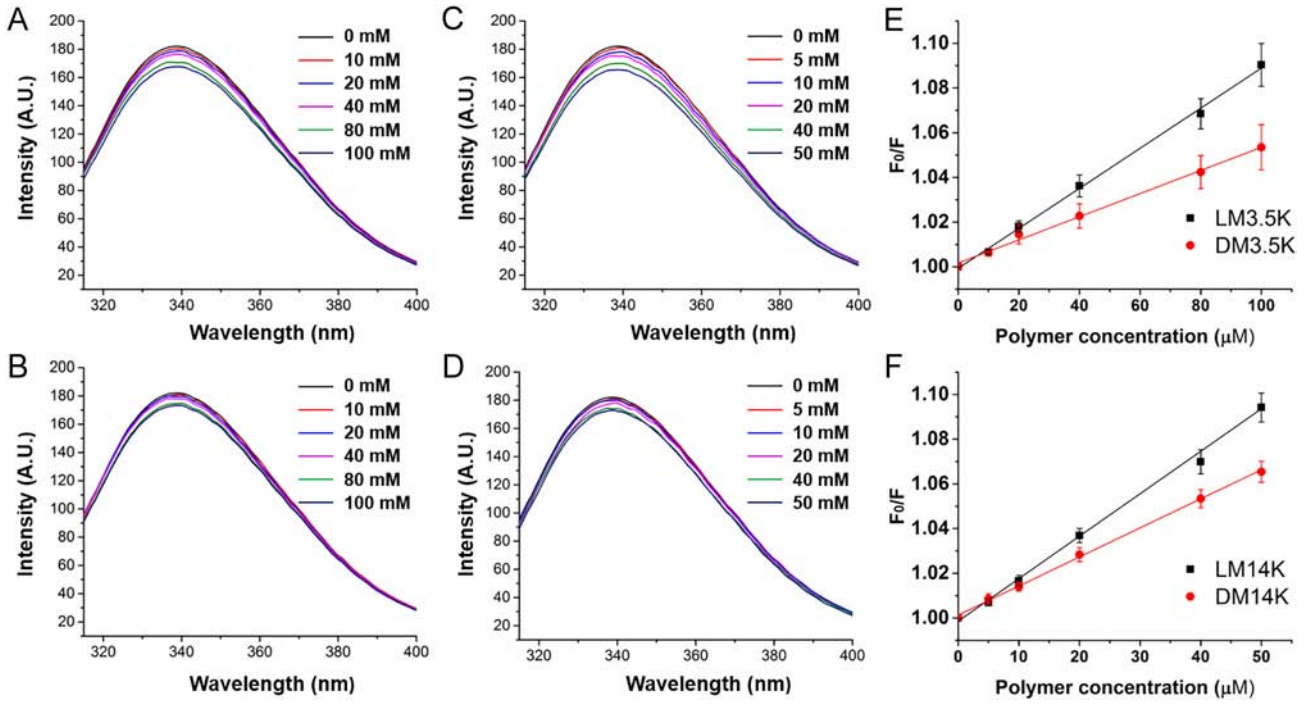

Figure 4. Micelle-BSA interactions measured by a fluorescence quenching assay. The fluorescence spectra of BSA (5 μM) in the presence of various concentrations of LM3.5 K **(A)**, DM3.5 K **(B)**, LM14K **(C)**, and DM14K **(D)** micelles. Stern-Volmer plots for tryptophan quenching by LM3.5 K and DM3.5 K micelles **(E)** and LM14K and DM14K micelles **(F)**. Results are presented as average ± S.D. (n = 3).

Table 4
Stern-Volmer quenching constant (K_{sv}) of tested micelles and G4 PAMAM dendrimer.

Micelles or polymers	K_{sv} (mM^{-1})	K_{sv} (mL/g)
LM3.5 K	0.90 ± 0.16	110.17 ± 19.61
DM3.5 K	0.52 ± 0.16	62.89 ± 18.84
LM14K	1.86 ± 0.23	99.54 ± 11.25
DM14K	1.21 ± 0.14	63.10 ± 7.62
G4 PAMAM	6.14 ± 0.49	432.15 ± 34.78

interactions and reduce the disassembly of the micelles, potentially decreasing uncontrolled drug release caused by this undesired interaction.

In vitro doxorubicin release study

In this *in vitro* release study, doxorubicin (DOX) was encapsulated in the micelles since it is a commonly used chemotherapeutic drug molecule with a fluorescence property. The loading efficiencies of all micelles tested were within a comparable range (75–85%), and the DOX loading did not significantly change the hydrodynamic diameters of the micelles (Table S1). The release profiles of DOX were obtained using a dialysis method in 50% FBS and 1% Tween 80 to evaluate the effect of dendritic polymer architecture on DOX release in the presence and absence of serum proteins.

Figure 3, *A* shows the DOX release profiles of DMs and LMs, which follows the same trend observed in the FRET-based stability study shown in Figure 2, *B*. The size of the PCL segment is still the dominant factor that determined the DOX release rate. At 12 h, the amount of DOX released from the micelles with PCL3.5 K is approximately 30% higher than that from the micelles with PCL14K (73–79% *vs.* 55–63%). At the same time point, the amounts of DOX released from DM3.5 K and DM14K are approximately 6% and 8% lower compared to LM3.5 K and LM14K, respectively. The difference between DMs and LMs is not as significant as what was observed in the FRET-based study. This could be attributed to the experimental setting of the release study. Considering that the release study was performed using a dialysis method, once the DOX molecules were released from the micelles, the free DOX would still need to diffuse through the dialysis membrane to be detected. This extra diffusion step could lessen the difference between groups. Interestingly, when the release study was performed in a protein-free medium containing 1% Tween 80 to solubilize free DOX, the difference between DMs and LMs was diminished (Figure 3, *B*). Under this condition, the PCL length became the only factor that affected the release rate. These results indicate that the slower DOX release from DMs only in 50% FBS is likely due to the reduction in micelle-serum protein interactions implemented by the dendritic architecture.

Micelle-serum albumin interactions

The BSA fluorescence quenching analysis is a commonly used method to study interactions of BSA with small molecules.[40,41] The tryptophan residues in BSA exhibit a characteristic fluorescence emission peak at around 340 nm, which is highly sensitive to changes in its surrounding environment. Hence, the changes of BSA fluorescence spectra

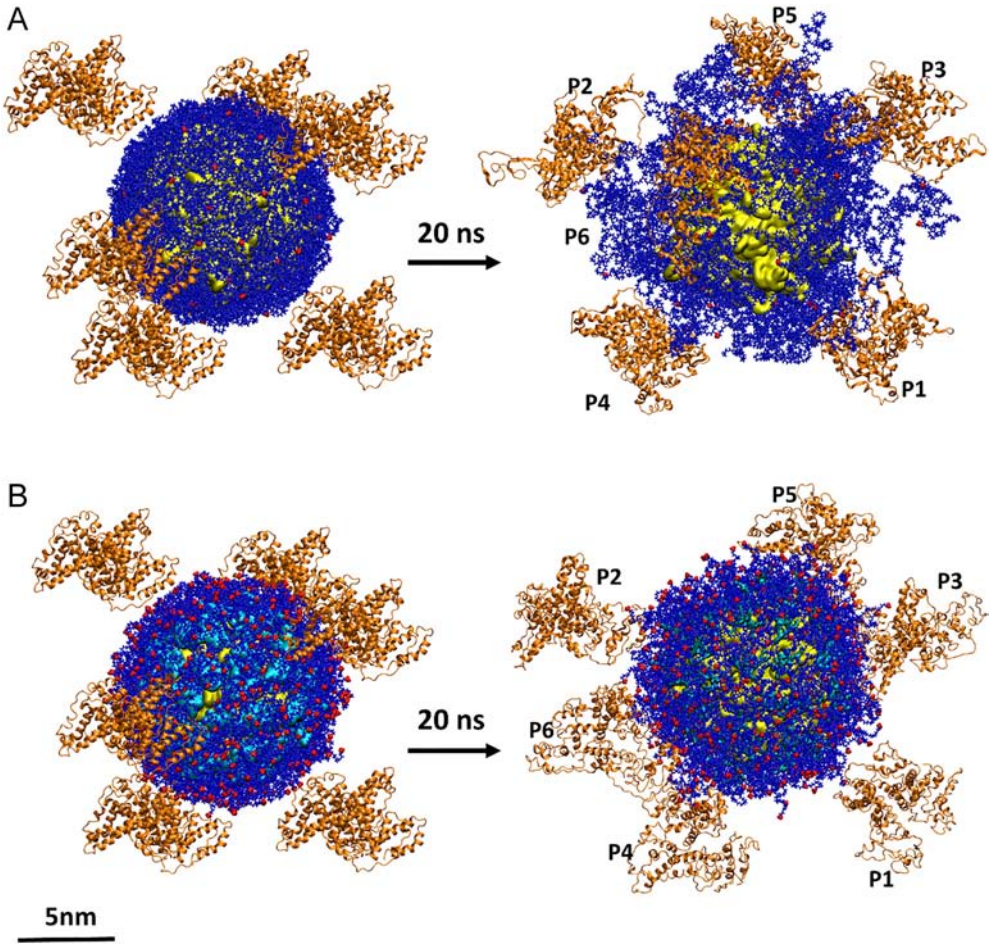

Figure 5. Atomistic MD simulations of the interaction between BSA and an LM3.5 K **(A)** or a DM3.5 K **(B)** micelle in an ionic solution (150 mM NaCl) at 0 ns and 20 ns of the simulation. (PCL is yellow; G3 dendron is cyan; PEG is blue; terminal methoxy group is red; BSA is orange). Scale bar: 5 nm.

could be used to evaluate the conformational changes of BSA upon their interaction with small molecules. This technique has also been employed to evaluate the interactions between BSA and various nanomaterials, such as surface modified dendrimers, dendritic polyglycerol and self-aggregated NPs.[42–44] We therefore employed this assay to analyze interactions between BSA and the micelles. To perform this quenching assay, DMs and LMs at various concentrations were mixed with BSA solution, followed by monitoring the fluorescence spectra of BSA.

In Figure 4, *A-D*, both DMs and LMs led to a concentration-dependent reduction of the tryptophan fluorescence, indicating that the interactions between micelles and BSA induce a conformational change of BSA. To quantify the quenching effect, the fluorescence data were analyzed using the Stern-Volmer equation (Eq. (3), see the experimental section) to calculate the quenching constant of each micelle. The calculated Stern-Volmer quenching constants of all four micelles are listed in Table 4. A generation 4 poly(amidoamine) (G4 PAMAM) dendrimer group was added as a positive control since PAMAM dendrimers with surface amine groups (-NH_2) are known to strongly interact with BSA due to electrostatic interactions.[44] In addition, because the molecular weights of the amphiphilic copolymers with short and long PCL chains are considerably different, we converted the unit of quenching constant from mM^{-1} to mL/g to better normalize the molecular weight differences. After this conversion, the Stern-Volmer quenching constants of all the tested micelles were below 111 mL/g, which was significantly lower than that of G4 PAMAM dendrimers (432.15 mL/g). Because all the micelles are protected by PEG outer shells, it is not surprising that the micelle-BSA interactions are substantially weaker than the positively charged dendrimers. The quenching constants of DM3.5 K and DM14K micelles were 62.89 ± 18.84 mL/g and 63.10 ± 7.62 mL/g, respectively, which were significantly lower than those from LMs (around 100 mL/g). The lower quenching constants of DMs further confirm that the dendritic PEG outer shells of DMs reduce the interactions between the micelles and serum albumins.

Molecular dynamics (MD) simulations

Next, atomistic MD simulations were performed to further understand the interactions of BSA with DMs and LMs in greater detail. Due to our limited computational capacity, only LM3.5 K and DM3.5 K were modeled. Six BSA molecules with different (random) orientations were placed on the surface of

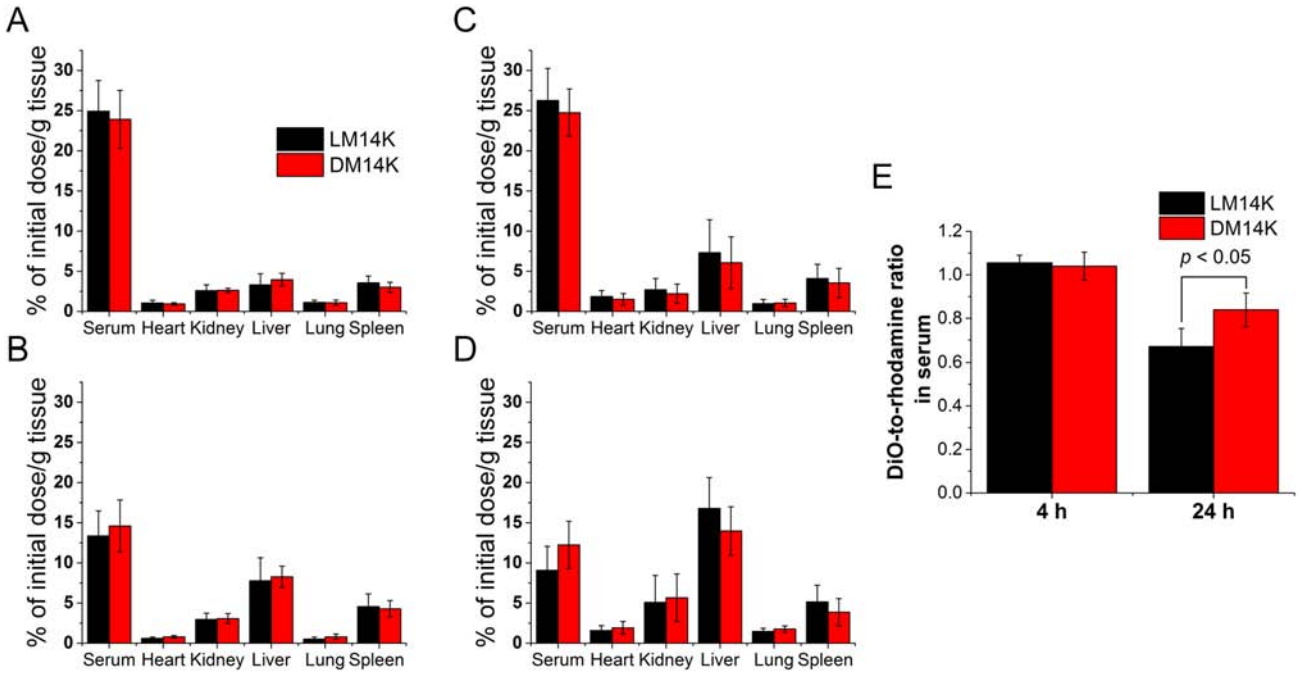

Figure 6. Biodistribution study of the dual-labeled (DiO-loaded, rhodamine-labeled) micelles. Dual-labeled LM14K and DM14K micelles (10 mg/kg) were injected *via* tail vein into mice. The blood and major organs of mice were collected at 4-h and 24-h post-injection for analysis. The biodistribution of rhodamine-labeled polymers at 4-h **(A)** and 24-h **(B)** post-injection. The biodistribution of DiO at 4-h **(C)** and 24-h **(D)** post-injection. **(E)** The DiO-to-rhodamine ratio in the mouse serum at 4-h and 24-h post-injection. Results are presented as average ± S.D. (n = 5).

LM3.5 K and DM3.5 K micelles in a 150 mM NaCl solution. Figure 5, *A* and *B* display the simulated LM3.5 K and DM3.5 K, respectively. The results show that the relaxed 5000 g/mol PEG chains of LM3.5 K form a diffused PEG outer shell through which BSA molecules can penetrate. In contrast, dendritic 600 g/mol PEG chains of PDCs form a dense PEG outer shell on DM3.5 K, blocking penetration of BSA.

To quantitatively measure the strength of micelle-BSA coupling, the van der Waals (vdW) and electrostatic coupling energies between BSA molecules and micelles were approximately evaluated from these simulation results. The average interaction energy of BSA to DM3.5 K (Figure S5) was about three times lower than that of LM3.5 K (LM3.5 K: -78.5 kcal/mol *vs.* DM3.5 K: -19.6 kcal/mol), indicating that dendritic PEG outer shell reduces the micelle-BSA interactions. Interestingly, the coupling energies between BSA and the PCL core were -0.1 kcal/mol for LM3.5 K *vs.* -0.3 kcal/mol for DM3.5 K, suggesting that both PEG outer shells could efficiently isolate the hydrophobic core from BSA (Figure S6). However, the diffused linear PEG outer shell allowed much greater micelle-BSA shell interaction as compared to the dendritic PEG outer shell (LM3.5 K: -78.4 kcal/mol *vs.* DM3.5 K: -19.3 kcal/mol), which results in stronger BSA interactions of LMs (Figure S6).

In vivo biodistribution study

The dual-labeled micelles were prepared by incorporating 0.3 wt% DiO into rhodamine-conjugated polymers during the self-assembly process. Given their relatively high serum stability, we only compared dual-labeled LM14K and DM14K. The dual-labeled micelles were administrated by the tail vein I.V. injection (10 mg/kg) into BALB/c mice. At 4-h or 24-h post-injection, the mice were euthanized and their blood and major organs (heart, kidney, liver, lung, and spleen) were collected for analysis.

Figure 6, *A* and *B* show the biodistribution of rhodamine-labeled micelles at 4-h and 24-h post-injection, respectively. At both time points, no significant differences in biodistribution were observed between DMs and LMs, indicating that the incorporation of dendritic architecture did not significantly alter the blood level and tissue distribution of the micelles. In contrast, when DiO was encapsulated in DM14K, a higher DiO content in the blood was observed and yet lower mononuclear phagocyte system (MPS) accumulation (liver and spleen) of DiO was detected at 24-h post-injection (Figure 6, *C* and *D*). Because free long-chain dialkylcarbocyanine probes (*e.g.* DiO) have been reported to accumulate in the MPS organs,[45] our results suggest that the dendritic PEG outer shell of DM14K likely prevents a fast DiO release in the blood stream and thus reduces the accumulation of free DiO in the MPS organs. However, the differences were not statistically significant due to the inter-subject variability. To minimize the inter-subject variability, we normalized the DiO content in the blood by the rhodamine content of the same sample and presented the data as the DiO-to-rhodamine ratio. As shown in Figure 6, *E*, although the DiO and rhodamine contents in serum fluctuated among mice, the ratio between DiO and rhodamine contents was constantly close to 1 at 4-h post-injection. This result indicates that most likely DiO was still encapsulated in both DMs and LMs at this point, so the relative contents between DiO and rhodamine-labeled polymers in the serum were nearly 1:1. As the encapsulated DiO was

released from the circulating micelles and accumulated in the MPS organs, these ratios dropped to 0.67 and 0.83 for LM14K and DM14K, respectively, at 24-h post-injection. The ratio for DM14K was higher (by 23%) than that for LM14K, which was statistically significant ($p < 0.05$). This result clearly demonstrates that the dendritic PEG outer shell of DMs reduces the uncontrolled release of hydrophobic molecules in the micelles in the blood stream, which may result in DM14K maintaining a higher blood level of the carried drugs *in vivo* for a longer period of time. This can be most likely attributed to the weaker micelle-serum protein interactions and greater micelle serum stability of DMs demonstrated in the earlier *in vitro* studies.

Discussion

We present herein a systematic study on the effect of dendritic polymer architecture on biological behaviors of the resulting micelles using a series of theoretical, *in vitro*, and *in vivo* experiments. PDCs and LBCs with comparable molecular weights were synthesized to form self-assembled micelles configured with either a short dendritic PEG or a long linear PEG outer shell. This design minimized any potential effect from other physical parameters than structural factors on the properties of self-assembled micelles for these polymers, allowing us to focus on the effect of polymeric architecture (dendritic *vs.* linear) on micelle-serum protein interactions. It has been reported that the dendritic polymer architecture positively affects the thermodynamic stability of polymeric micelles, likely attributed to its conical (dendron) structure, pre-organized to form a micelle with a minimal entropy cost.[24] The same phenomenon was observed in this study, as DMs exhibited lower CMCs than LMs with the same length of the hydrophobic segment (Table 2). However, the thermodynamic stability based on CMC does not necessarily dictate the stability of self-assembled NPs in physiological environments, where the micelles encounter numerous serum proteins during systematic circulation, which could potentially disintegrate them and cause premature drug release even when the concentrations of micelles are above their CMCs.[46] Therefore, the FRET technique was employed to further investigate the influence of dendritic polymer architecture on the micelle stability upon the interactions with serum proteins. The FRET-based micelle stability study demonstrates that DMs exhibited a significantly slower micelle disintegration rate in the presence of serum proteins. One can still argue that an increase in the length of hydrophobic PCL chain would likely enhance the serum stability of the resulting micelle due to increased hydrodynamic stability of micelles (*i.e.*, reduced CMCs). While the incorporation of dendritic polymer architecture marginally decreased CMCs by 20–30% (Table 2), however, it significantly prolonged the half-life of micelles in the serum-containing media by approximately 2-fold (Table 3). These findings suggest that the dendritic PEG outer shell plays a more important role in reducing the micelle-serum protein interactions, which minimizes the uncontrolled drug release of thermodynamic stable micelles in the presence of serum proteins. This statement is further supported by the *in vitro* DOX release study. In a serum-containing medium, the superior serum stability of DMs was translated into a slower drug release profile when compared to their linear counter parts. On the other hand, DMs and LMs showed similar release profiles in a serum-free medium, suggesting that the dendritic PEG outer shell itself does not slow down the outbound diffusion of the encapsulated drugs. Therefore, the slower drug release kinetics of DMs in the serum-containing medium could be mainly attributed to the less micelle-serum protein interactions.

To obtain mechanistic understanding of these behaviors of the micelles, we performed a fluorescence quenching analysis and MD simulations to directly compare the interactions between BSA, the major component of serum proteins, and the micellar NCs. While the BSA quenching assay indicates that the dendritic PEG outer shell induces a lower degree of BSA conformational change, the MD simulations further demonstrate that the dendritic PEG design prevents the penetration of the serum proteins into the micelle and thus results in their lower binding energies. Taken together, both studies suggest that the dense dendritic PEG outer shell reduces the micelle-serum protein interactions more effectively than the linear PEG outer shell.

Finally, we studied the *in vivo* tissue distribution of dual-labeled DMs and LMs to figure out if the incorporation of dendritic polymer architecture leads to different biodistributions of the self-assembled NCs and the carried drugs. Although our results show that the dendritic PEG outer shell did not substantially alter the biodistribution of the micelles in the *in vivo* study, it reduced the uncontrolled release of the encapsulated molecules, which is often caused by non-specific micelle-serum protein interactions.

In summary, the improved serum stability and *in vitro* DOX release profiles of DMs collectively demonstrate, for the first time to our knowledge, that the dendritic polymer architecture allows micelles to better withstand the negative influence of micelle-serum protein interactions. With slightly lower CMCs, the DMs exhibited ~2-fold longer half-life in serum-containing media compared to their LM counterparts, suggesting that the dendritic PEG outer shell of DMs significantly reduces micelle-serum protein interactions. In addition to the fluorescence quenching analysis demonstrating the ability of the dendritic PEG outer shell in suppressing micelle-serum protein interactions, the MD simulations reveal that the dendritic PEG outer shell prevents the penetration of serum proteins in the micelles and thus weakens the protein binding. When being tested *in vivo*, this dendritic design is shown to reduce the premature release of the encapsulated molecules from the micelles. All of these results support that dendritic polymer architecture provides enhanced serum stability of micelles, which is a desired biological property of NCs. As our previous work has suggested that the dendritic polymer architecture improves the thermodynamic stability of micelles, this work further demonstrates that this design reduces unwanted non-specific interactions with serum proteins. Our results herein suggest a novel approach that can be potentially applied for a variety of self-assembled NPs to promote their effectiveness in drug delivery.

Acknowledgments

This work was partially supported by National Science Foundation (NSF) under grant # DMR-1409161/1709173 and by

National Institutes of Health (NIH) under grant # 1R01CA182528 and 1R21EB022374. P.K. acknowledges the support from NSF DMR-1506886 grant.

Appendix A. Supplementary data

Supplementary data to this article can be found online at https://doi.org/10.1016/j.nano.2018.05.010.

References

1. Lee CC, MacKay JA, Frechet JMJ, Szoka FC. Designing dendrimers for biological applications. *Nat Biotechnol* 2005;**23**(12):1517-26.
2. Peer D, Karp JM, Hong S, Farokhzad OC, Margalit R, Langer R. Nanocarriers as an emerging platform for cancer therapy. *Nat Nanotechnol* 2007;**2**(12):751-60.
3. Duncan R. The dawning era of polymer therapeutics. *Nat Rev Drug Discov* 2003;**2**(5):347-60.
4. Wurm F, Frey H. Linear-dendritic block copolymers: the state of the art and exciting perspectives. *Prog Polym Sci* 2011;**36**(1):1-52.
5. Gu FX, Karnik R, Wang AZ, et al. Targeted nanoparticles for cancer therapy. *Nano Today* 2007;**2**(3):14-21.
6. van der Meel R, Vehmeijer LJ, Kok RJ, Storm G, van Gaal EV. Ligand-targeted particulate nanomedicines undergoing clinical evaluation: current status. *Adv Drug Deliv Rev* 2013;**65**(10):1284-98.
7. Chauhan VP, Jain RK. Strategies for advancing cancer nanomedicine. *Nat Mater* 2013;**12**(11):958-62.
8. Pearson RM, Hsu H-j, Bugno J, Hong S. Understanding nano-bio interactions to improve nanocarriers for drug delivery. *MRS Bull* 2014;**39**(3):227-37.
9. Cedervall T, Lynch I, Lindman S, et al. Understanding the nanoparticle–protein corona using methods to quantify exchange rates and affinities of proteins for nanoparticles. *Proc Natl Acad Sci* 2007;**104**(7):2050-5.
10. Pearson RM, Juettner VV, Hong S. Biomolecular corona on nanoparticles: a survey of recent literature and its implications in targeted drug delivery. *Front Chem* 2014;**2**:108.
11. Kim S, Shi Y, Kim JY, Park K, Cheng J-X. Overcoming the barriers in micellar drug delivery: loading efficiency, in vivo stability, and micelle-cell interaction. *Expert Opin Drug Deliv* 2010;**7**(1):49-62.
12. Dai Q, Walkey C, Chan WC. Polyethylene glycol backfilling mitigates the negative impact of the protein corona on nanoparticle cell targeting. *Angew Chem Int Ed* 2014;**53**(20):5093-6.
13. Salvati A, Pitek AS, Monopoli MP, et al. Transferrin-functionalized nanoparticles lose their targeting capabilities when a biomolecule corona adsorbs on the surface. *Nat Nanotechnol* 2013;**8**(2):137-43.
14. Pearson RM, Sen S, H-j Hsu, et al. Tuning the selectivity of Dendron micelles through variations of the poly (ethylene glycol) corona. *ACS Nano* 2016;**10**(7):6905-14.
15. Chen H, Kim S, Li L, Wang S, Park K, Cheng J-X. Release of hydrophobic molecules from polymer micelles into cell membranes revealed by Förster resonance energy transfer imaging. *Proc Natl Acad Sci* 2008;**105**(18):6596-601.
16. Owen SC, Chan DP, Shoichet MS. Polymeric micelle stability. *Nano Today* 2012;**7**(1):53-65.
17. Oerlemans C, Bult W, Bos M, Storm G, Nijsen JF, Hennink WE. Polymeric micelles in anticancer therapy: targeting, imaging and triggered release. *Pharm Res* 2010;**27**(12):2569-89.
18. Deng C, Jiang Y, Cheng R, Meng F, Zhong Z. Biodegradable polymeric micelles for targeted and controlled anticancer drug delivery: promises, progress and prospects. *Nano Today* 2012;**7**(5):467-80.
19. Cabral H, Kataoka K. Progress of drug-loaded polymeric micelles into clinical studies. *J Control Release* 2014;**190**:465-76.
20. Biswas S, Kumari P, Lakhani PM, Ghosh B. Recent advances in polymeric micelles for anti-cancer drug delivery. *Eur J Pharm Sci* 2016;**83**:184-202.
21. Perry JL, Reuter KG, Kai MP, et al. PEGylated PRINT nanoparticles: the impact of PEG density on protein binding, macrophage association, biodistribution, and pharmacokinetics. *Nano Lett* 2012;**12**(10):5304-10.
22. H-j Hsu, Sen S, Pearson RM, Uddin S, Král P, Hong S. Poly (ethylene glycol) corona chain length controls end-group-dependent cell interactions of dendron micelles. *Macromolecules* 2014;**47**(19):6911-8.
23. Logie J, Owen SC, McLaughlin CK, Shoichet MS. PEG-graft density controls polymeric nanoparticle micelle stability. *Chem Mater* 2014;**26**(9):2847-55.
24. Bae JW, Pearson RM, Patra N, et al. Dendron-mediated self-assembly of highly PEGylated block copolymers: a modular nanocarrier platform. *Chem Commun* 2011;**47**(37):10302-4.
25. Pearson RM, Patra N, Hsu H-j, Uddin S, Král P, Hong S. Positively charged dendron micelles display negligible cellular interactions. *ACS Macro Lett* 2012;**2**(1):77-81.
26. Lu J, Owen SC, Shoichet MS. Stability of self-assembled polymeric micelles in serum. *Macromolecules* 2011;**44**(15):6002-8.
27. Phillips JC, Braun R, Wang W, et al. Scalable molecular dynamics with NAMD. *J Comput Chem* 2005;**26**:1781-802.
28. MacKerell Jr AD, Bashford D, Bellott M, et al. All-atom empirical potential for molecular modeling and dynamcis studies of proteins. *J Phys Chem B* 1998;**102**:3586-616.
29. MacKerell Jr AD, Feig M, Brooks CL. Extending the treatment of backbone energetics in protein force fields: limitations of gas-phase quantum mechanics in reproducing protein conformational distributions in molecular dynamics simulations. *J Comput Chem* 2004;**25**:1400-15.
30. Vanommeslaeghe K, Hatcher E, Acharya C, et al. CHARMM general force field: a force field for drug-like molecules compatible with the CHARMM all-atom additive biological force field. *J Comput Chem* 2010;**31**:671-90.
31. Vanommeslaeghe K, Raman EP, MacKerell Jr AD. Automation of the CHARMM general force field (CGenFF) II: assignment of bonded parameters and partial atomic charges. *J Chem Inf Model* 2012;**52**:3155-68.
32. Yu W, He X, Vanommeslaeghe K, MacKerell Jr AD. Extension of the CHARMM general force field to sulfonyl-containing compounds and its utility in biomolecular simulations. *J Comput Chem* 2012;**33**:2451-68.
33. Darden T, York D, Pedersen L. Particle mesh Ewald: an N·log(N) method for Ewald sums in large systems. *J Chem Phys* 1993;**98**(12):10089-92.
34. Humphrey W, Dalke A, Schulten K. VMD: visual molecular dynamics. *J Mol Graph* 1996;**14**(1):33-8.
35. Van Domeselaar GH, Kwon GS, Andrew LC, Wishart DS. Application of solid phase peptide synthesis to engineering PEO–peptide block copolymers for drug delivery. *Colloids Surf, B* 2003;**30**(4):323-34.
36. Ranger M, Jones MC, Yessine MA, Leroux JC. From well-defined diblock copolymers prepared by a versatile atom transfer radical polymerization method to supramolecular assemblies. *J Polym Sci A Polym Chem* 2001;**39**(22):3861-74.
37. Savic R, Azzam T, Eisenberg A, Maysinger D. Assessment of the integrity of poly (caprolactone)-b-poly (ethylene oxide) micelles under biological conditions: a fluorogenic-based approach. *Langmuir* 2006;**22**(8):3570-8.
38. Diezi TA, Bae Y, Kwon GS. Enhanced stability of PEG-block-poly(N-hexyl stearate l-aspartamide) micelles in the presence of serum proteins. *Mol Pharm* 2010;**7**(4):1355-60.
39. Miller T, Rachel R, Besheer A, Uezguen S, Weigandt M, Goepferich A. Comparative investigations on in vitro serum stability of polymeric micelle formulations. *Pharm Res* 2012;**29**(2):448-59.
40. Peters Jr T. *All About Albumin: Biochemistry, Genetics, and Medical Applications*. Academic press; 1995.

41. Abou-Zied OK, Al-Shihi OI. Characterization of subdomain IIA binding site of human serum albumin in its native, unfolded, and refolded states using small molecular probes. *J Am Chem Soc* 2008;**130**(32):10793-801.
42. Wang Y, Jiang Q, Liu LR, Zhang Q. The interaction between bovine serum albumin and the self-aggregated nanoparticles of cholesterol-modified O-carboxymethyl chitosan. *Polymer* 2007;**48**(14):4135-42.
43. Khandare J, Mohr A, Calderón M, Welker P, Licha K, Haag R. Structure-biocompatibility relationship of dendritic polyglycerol derivatives. *Biomaterials* 2010;**31**(15):4268-77.
44. Klajnert B, Stanisławska L, Bryszewska M, Pałecz B. Interactions between PAMAM dendrimers and bovine serum albumin. *Biochim Biophys Acta Proteins Proteomics* 2003;**1648**(1):115-26.
45. Attia ABE, Yang C, Tan JP, et al. The effect of kinetic stability on biodistribution and anti-tumor efficacy of drug-loaded biodegradable polymeric micelles. *Biomaterials* 2013;**34**(12):3132-40.
46. Chen H, Kim S, He W, et al. Fast release of lipophilic agents from circulating PEG-PDLLA micelles revealed by in vivo forster resonance energy transfer imaging. *Langmuir* 2008;**24**(10):5213-7.